Chinese Chemical Letters 32 (2021) 1462–1465

Contents lists available at ScienceDirect

Chinese Chemical Letters

journal homepage: www.elsevier.com/locate/cclet

Communication

Magnetic beads-based multicolor colorimetric immunoassay for ultrasensitive detection of aflatoxin B_1

Shan He[a], Qitong Huang[b], Ying Zhang[a], Huifang Zhang[a], Huifeng Xu[c,**], Xun Li[a,**], Xiaoming Ma[a,d,*]

[a] Department of Chemistry and Chemical Engineering, Gannan Normal University, Ganzhou 341000, China
[b] Scientific Research Center, Gannan Medical University, Ganzhou 341000, China
[c] Fujian Key Laboratory of Integrative Medicine on Geriatrics, Academy of Integrative Medicine, Fujian University of Traditional Chinese Medicine, Fuzhou 350100, China
[d] State Key Laboratory of Chemo/Biosensing and Chemometrics, Hunan University, Changsha 410082, China

ARTICLE INFO

Article history:
Received 27 June 2020
Received in revised form 4 August 2020
Accepted 25 September 2020
Available online 28 September 2020

Keywords:
Mycotoxin
Aflatoxin B_1
Magnetic beads
Immunoassay
Multicolor
Colorimetry

ABSTRACT

Aflatoxin B_1 (AFB_1) is one of the most toxic, mutagenic and carcinogenic mycotoxin, widely exists in contaminated food, grains and feedstuff products. In this study, a novel magnetic beads multicolor colorimetric immunoassay (MBMCIA) based on Au@Ag nanorods (Au@Ag NRs) is proposed to visual detect ultralow concentration of AFB_1 with high-resolution by the naked-eye. To design the MBMCIA system, AFB_1-BSA conjugates were first coated on the surface of magnetic beads (MBs), then alkaline phosphatase (ALP) as a bridge between immunoassay and color reaction was used for catalytic hydrolysis of ascorbic acid-phosphate to generate reductive ascorbic acid. Finally, the yielded ascorbic acid could reduce silver ions to grow a silver coating on the surface of gold nanorods to generate Au@Ag NRs, which leads to the bule-shifted longitudinal absorption peak of Au NRs, accompanying with a series of perceptible color change. Under the optimal conditions, the proposed MBMCIA exhibited good sensitivity and specificity for the detection of AFB_1 with the detection limit as low as 5.7 pg/mL. Meanwhile, the MBMCIA was also applied for the analysis of AFB_1 in spiked wheat samples, the obtained recoveries range from 99.1% to 104.3% with relative standard deviation (RSD) less than 7.05% were acceptable. The proposed MBMCIA integrates separated, enriched, anti-interference and signal read-out into one, which opens up a new avenue for an on-site visual food safety inspection or environmental monitoring.

Aflatoxins are highly toxic secondary metabolites produced mainly by *Aspergillus flavus* and *Aspergillus parasiticus*, which have been proven to be potent teratogens, mutagenic and carcinogens [1–3]. Numerous researches have provided evidence that excessive aflatoxins can cause harm to normal liver tissues/organs and even closely related to human diseases such as liver cancer and stomach cancer [4]. Aflatoxin B_1 (AFB_1) is recognized as one of the most toxic and carcinogenic mycotoxins, widely exists in various agriculture products and vegetable oils (such as peanut, maize, and oilseeds) [5,6]. Because of its spread distribution and perniciousness, aflatoxin B_1 is classified as a Group I human carcinogen in 1993 by the International Agency for Research on Cancer (IARC) [7]. Furthermore, the stability of the AFB_1 was good in light, acid and heat conditions, which result in the AFB_1 cannot be destroyed by ordinary cooking (the crack temperature at 268 °C) and cause some harmful effects to human health [8]. More importantly, many countries have established limits on AFB_1 levels in agriculture products and vegetable oils, thereby it is urgently needed to develop a simple, rapid and visual detection method for AFB_1 detection to ensure the safety of agricultural products import and export.

Traditional analytical methods for the AFB_1 detection mainly include high-performance liquid chromatography (HPLC) [9], thin layer chromatography (TLC) [10], liquid chromatography-mass spectrometry (LC–MS/MS) [11]. Although these traditional methods have good accuracy and high selectivity, they require complicated sample preparation, time-consuming, expensive equipment, and professional skills. For simple and rapid detection of AFB_1, numerous studies focus on the antibody-based immunoassay technologies have been reported [12], such as enzyme-

* Corresponding author at: Department of Chemistry and Chemical Engineering, Gannan Normal University, Ganzhou 341000, China.
** Corresponding authors.
E-mail addresses: xuhf@fjtcm.edu.cn (H. Xu), gnsylixun@163.com (X. Li), maxlovery@163.com (X. Ma).

https://doi.org/10.1016/j.cclet.2020.09.047
1001-8417/

linked immunosorbent assay (ELISA) [13], immunochromatographic strip-test [14], fluorescence polarization immunoassay [15], photoelectrochemical immunoassay [16] and electrochemical immunoassay [17]. Among them, the microplate-based ELISA is the most widely used immunoassay method for target detection because of its universality, simplicity and cost-effectiveness. But microplate-based ELISA requires prolonged incubation time, tedious washing steps, and poor visual detection sensitivity, which limits its practical applications for on-site detection and screening of target. Compared with the microplate-based ELISA, the magnetic beads enzyme-linked immunoassay provides simple operation, high flexibility, fast speed, good portability and high sensitivity [18,19]. This is mainly because the large specific surface area and rich surface functionalization groups of magnetic beads (MBs), which are immobilized with a great number of substances such as antibodies, oligonucleotides and small molecules [20]. In addition, the MBs can easily separate and enrich analytes from complex solutions with the assistance of an external magnetic [21–23].

Recently, most of the reported chromogenic substrates (*e.g.*, 3,3′,5,5′-tetramethylbenzidine (TMB), 2,2′-azino-bis(3-ethylbenzothiazoline-6-sulfonic acid) (ABTS) and 4-nitrophenylphosphate (pNPP)) are widely used in the conventional colorimetric ELISA [24–26]. However, the color only showed the monochromic color change in response to different concentrations of targets and cannot quantitative detection with the naked eye. It is known to all that the multicolor changes are easier to be distinguished by human eyes than optical density changes of the single color [27]. According to the literature, gold nanorods (Au NRs) are used as multicolor chromogenic substrates due to their unique localized surface plasmon resonance (LSPR) absorption properties and high molar extinction coefficient [28–31]. For example, Xiong and his colleagues reported a highly sensitive colorimetric immunoassay based on the enzyme-assisted etching of Au nanorods for detection aflatoxin B_1 in corn samples [32]. However, this method of etching Au NRs suffers from severe challenges due to its low color resolution and long etching time. Recent studies have been shown that enzyme-mediated deposition of silver nanoshells on the surface of Au NRs resulted in a decrease in the aspect ratio of Au NRs and multicolor change [33,34]. This feature has been successfully used for sensitive colorimetric detection of cancer biomarkers [35], enzyme activity [33,36] and food freshness [37]. However, the application of the fascinating phenomenon for the detection of food contaminants in food samples is still scarce.

Herein, we proposed a novel magnetic beads multicolor colorimetric immunoassay (MBMCIA) for simple and high color resolution detection of food contamination AFB_1 *via* integrated magnetic beads with the alkaline phosphatase (ALP)-mediated silver deposition on the Au NRs into immunoassay. The MBMCIA merged four functional components: MBs for enriching biomarkers, Au NRs for multicolor chromogenic substrate, anti-AFB_1 monoclonal antibody for specific recognizer, and ALP for the bridge between immunoassay and chromogenic reaction. This suggested immunoassay is accordingly capable of recognition, separation, enrichment, and onsite visual analysis of target AFB_1. More interestingly, the concentration of target AFB_1 could be easily distinguished with the naked eye due to high-resolution multiple color changes of Au NRs. As a consequence, the proposed MBMCIA may have a great potential application for on-site detection and screening in real samples due to its portability and easy visualization.

In this work, the mechanism of the proposed MBMCIA for the detection of AFB_1 was elucidated in Scheme 1. The carboxyl groups on magnetic beads were initially activated through 1-ethyl-3-(3-dimethyllaminopropyl)carbodiimide hydrochloride (EDC) and *N*-hydroxysuccinimide (NHS), then coupled with the amino groups of

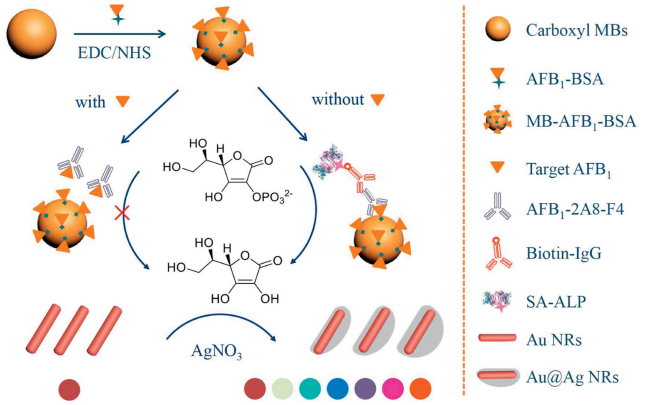

Scheme 1. Schematic illustration of the proposed MBMCIA for ultrasensitive detection of AFB_1 based on Au@Ag nanorods.

albumin from bovine serum albumin (BSA) by the caprylic acid-ammonium sulfate reaction to form MBs-AFB_1-BSA. When the target AFB_1 is present, AFB_1 compete with AFB_1-BSA to preferentially recognize the anti-AFB_1 monoclonal antibodies (AFB_1-2A8-F4), resulting in inevitably decrease of the captured biotin-labeled antibody (Biotin-IgG) and streptavidin-conjugated alkaline phosphatase (SA-ALP), which cannot trigger the ALP-induced catalytic reaction. In contrast, in the absence of AFB_1, a large amount of anti-AFB_1 monoclonal antibodies and Biotin-IgG are immobilized on the surface of MBs by immunoreaction. Subsequently, SA-ALP is immobilized by biotin-avidin-system and triggers the subsequent catalytic and multicolor reaction. The ALP can catalytic hydrolyzes sodium L-ascorbic acid-2-phosphate (AA-P) to generate ascorbic acid (AA), the produced AA acted as a common reduction to reduce silver ions and consequent deposition of metallic silver on the Au NRs to generate Au@Ag NRs. This leads to both the blue-shifted of longitudinal LSPR peak and the decrease of the aspect ratio of Au NRs, accompanying a series of vivid multicolor changes from the initial reddish-brown to green, cyan, blue, violet, and further to orange. Therefore, the proposed MBMCIA based on ALP-mediated silver deposition on the Au NRs transforms the insensitive traditional signal-color change into a distinguishable multicolor change.

To confirm the mechanism of ALP-mediated silver deposition on the Au NRs, a series of control experiments were carried out and recorded by UV–vis spectroscopy and color change images. As shown in Figs. 1A and B, the Au NRs solution appears light reddish-brown (photograph 'a') and exhibits the transverse and longitudinal LSPR absorption peaks at 509 nm and 701 nm, respectively (curve a). In absence of ALP, the color of Au NRs colloids solution was not changed (photographs b, c and d) and the longitudinal LSPR peaks of Au NRs were negligible shifted (curves b, c and d)

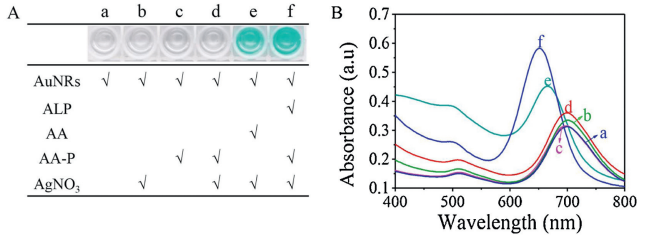

Fig. 1. (A) Photographs and (B) UV–vis absorption spectra of (a) Au NRs, (b) Au NRs + $AgNO_3$, (c) Au NRs + AA-P, (d) Au NRs + $AgNO_3$ + AA-P, (e) Au NRs + $AgNO_3$ + AA, and (f) Au NRs + ALP + $AgNO_3$ + AA-P. The concentrations of AA-P, $AgNO_3$, AA and ALP are 2.0 mmol/L, 4.0 mmol/L, 0.05 mmol/L and 100.0 mU/mL, respectively. The reaction time of silver nanoshells deposited on the surface of Au NRs was 60 min, with solution pH 9.8.

even if AA-P and $AgNO_3$ were added. When ALP, AA-P, and $AgNO_3$ were mixed with the Au NRs solution and incubated 60 min at 37 °C, the color of solution favorably changed from light reddish-brown to green (photograph f), and the longitudinal LSPR peak was gradually blue-shifted from 701 nm to 651 nm (curve f). After mixing Au NRs, $AgNO_3$, and AA, the color of the solution changed from light reddish-brown to green (photograph e) and the longitudinal LSPR peak gradually blue-shifted from 701 nm to 665 nm (curve e). The result demonstrates that the AA obtained by the hydrolysis of AA-P with the aid of ALP is the key factor for this method, and can reduce silver ions coating the surface of Au NRs to form Au@Ag NRs.

To further confirmed the formation of silver nanoshells on the Au NRs, the morphology and size changes of Au NRs were observed by transmission electron microscopy (TEM), the as-synthesized nanostructures were well-defined nanorods with an average length of 50 nm and a diameter of 16 nm (Fig. S1A in Supporting information). After adding ALP, AA-P, and $AgNO_3$ into the Au NRs solution, metallic silver was first deposited on the surface of Au NRs to form Au@Ag NRs nanostructures and the solution color turned to green (Fig. S1B in Supporting information). As the concentration of ALP increased, the silver nanoshells preferred to deposit on the transverse axis of Au NRs, resulting in the aspect ratio of Au NRs decreased and the color changed to blue (Fig. S1C in Supporting information). The final size of the as-produced was significantly larger than Au NRs and formed orange spherical-like nanostructures (Fig. S1D in Supporting information). Moreover, it is well known that the hybrid nanostructure could easily cause the blue-shift of the longitudinal LSPR peak due to its excellent optical properties and nanostructure.

To improve the visual detection accuracy, Au NRs was utilized as a chromogenic substrate for multicolor quantitative detection of the analytes. As shown in Scheme 1, food contaminant aflatoxin B_1 (AFB_1) was used as a model analyte and ALP was labeled on the second antibody by the avidin-biotin system. The number of SA-ALP that immobilized on the surface of MBs was decreased with the increasing concentration of AFB_1 in the samples. As a result, the amount of AA-P hydrolyzed by ALP was inversely proportional to the concentration of AFB_1 due to the indirect competitive immunoreaction. Under optimal conditions (Fig. S2 in Supporting information), the vivid color of the sample solution change from orange to purple-red to purple to blue and to green with the increase of AFB_1 concentration (Fig. 2A). The longitudinal LSPR intensity of the Au NRs was normalization such that one normalized unit to evaluate the AFB_1 concentration. As shown in Fig. 2B, the longitudinal LSPR peak of the Au NRs gradually red-shifted with the increasing AFB_1 concentration in the range of 0–10.0 ng/mL. Fig. 2C displayed a good linear correlation between blue-shifts of the longitudinal LSPR peak ($\Delta\lambda$) and AFB_1 concentrations in the dynamic range from 0.01 ng/mL to 10.0 ng/mL, and the linear regression equation could be fitted to y ($\Delta\lambda$) = −136.2C (ng/mL) + 164.7 with the correlation coefficient (R^2) of 0.9866. The limit of detection (LOD) was evaluated as low as 5.7 pg/mL based on 3σ/slope, where σ was the standard deviation of blank samples. Compared with other analytical methods for the detection of AFB_1, the proposed MBMCIA not only achieved higher sensitivity and lower LOD, but also possessed a unique advantage of semi-quantitative visual detection of the target with the naked eye [38–40] (Table S1 in Supporting information). Besides, the mechanism of ALP-mediated silver deposition on the Au NRs was also performed to visual detection of ALP activity in Fig. S3 (Supporting information).

To evaluate the selectivity of the proposed MBMCIA toward AFB_1 detection, four types of mycotoxins (*e.g.*, aflatoxin B_2 (AFB_2), aflatoxin G_1 (AFG_1), ochratoxin A (OTA), deoxynivalenol (DON)) were selected as interfering substances under the same experimental conditions. As shown in Fig. S4 (Supporting information), in the presence of target AFB_1, the blue-shifted of longitudinal LSPR peak ($\Delta\lambda$) only slightly changes due to the natural specificity of the antibody-antigen effect. In contrast, after adding above interference substances (concentration of mycotoxins were ten-fold higher than that of AFB_1), they were similar to the sample without AFB_1 that the longitudinal LSPR peaks of Au NRs were blue-shifted. The results demonstrate that the proposed MBMCIA shows high selectivity for accurate detection of AFB_1.

We also investigated the potential application of the proposed MBMCIA in real samples, spiked samples containing the wheat flour and different concentration of AFB_1 were tested. The MBs was used for the rapid separation and enrichment of target in the complex matrices without the purification process. As shown in Table 1, three spiked samples were investigated; the results showed that the recoveries range of 99.1%–104.3% and corresponding RSD range of 1.51%–7.05%, which indicates that the proposed MBMCIA has reliable accuracy and precision. These results show that the MBMCIA holds the potential applications for on-site visual detection and screening in food safety.

In summary, this study successfully develops a simple, convenient, ultrasensitive and high-resolution magnetic bead multicolor colorimetric immunoassay for the detection of AFB_1. Experimental results demonstrated that the proposed MBMCIA

Table 1
Recovery studies of AFB_1 spiked wheat flour samples ($n = 3$).

Spiked samples (ng/mL)	Mean (ng/mL)	Recovery (%)	RSD (%)
0.1	0.103	102.8	7.05
1.0	1.04	104.3	5.13
10.0	9.91	99.1	1.51

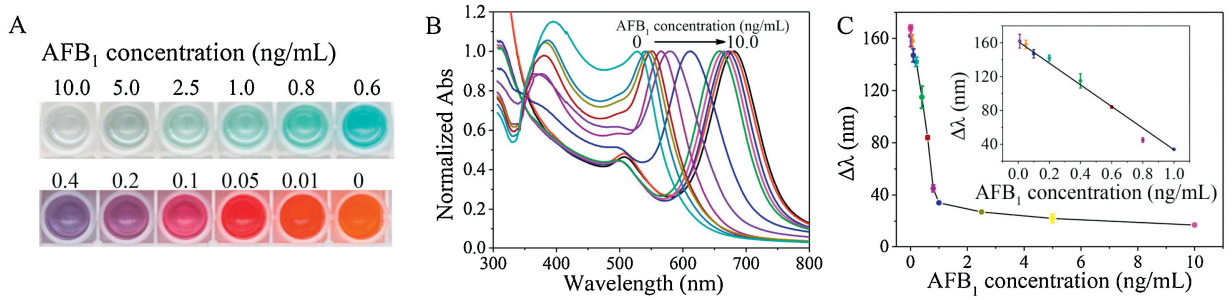

Fig. 2. (A) Photographs and (B) UV–vis absorption spectra of the proposed method toward AFB_1 with different concentrations (from left to right: 10.0, 5.0, 2.5, 1.0, 0.8, 0.6, 0.4, 0.2, 0.1, 0.05, 0.01, and 0 ng/mL). (C) The relationship between the longitudinal LSPR peak blue-shifted value ($\Delta\lambda$) and AFB_1 concentration (Inset: Linear curve). The concentrations of AA-P and $AgNO_3$ are 2.0 mmol/L and 4.0 mmol/L, respectively. The reaction time of silver nanoshells deposited on the surface of Au NRs was 60 min, with a solution pH of 9.8. Error bar represents the standard deviation ($n = 3$).

has the following advantages: (1) Magnetic beads replace microplates as an immobile phase to make the immunoreaction from two-dimensional to three-dimensional, further improve the sensitivity of the immunoassay and shorten the detection time. (2) The proposed multicolor method based on the silver nanoshells deposition on the surface of Au NRs provides a higher color resolution than those of colorimetric sensors based on aggregation or etching of Au NRs. (3) The MBMCIA has a series of advantages including simple, portable, visualization,high-sensitivity and on-site quantitative detection of AFB_1. Therefore, the proposed method provides a great possibility for the analysis of food contaminants in real samples.

Declaration of competing interest

The authors report no declarations of interest.

Acknowledgments

This work was supported by the National Natural Science Foundation of China (Nos. 21804022, 21964003 and 81773894), the Natural Science Foundation of Jiangxi Province (No. 20202BABL213019), the Science and Technology Project of the Education Department of Jiangxi Province of China (No. GJJ190775) and the Special Graduate Student Innovation Fund of Jiangxi Province (No. CX190013). This work was also supported by Open Project of Jiaxing University Key Laboratory of Rapid Detection Technology and Instruments for Environment and Food.

Appendix A. Supplementary data

Supplementary material related to this article can be found, in the online version, at doi:https://doi.org/10.1016/j.cclet.2020.09.047.

References

[1] Y. Lin, Y. Lin, D. Tang, et al., Biosens. Bioelectron. 74 (2015) 680–686.
[2] M. Masood, S.Z. Iqbal, M.R. Asi, N. Malik, Food Control 55 (2015) 62–65.
[3] C. Wang, L. Sun, Q. Zhao, Chin. Chem. Lett. 30 (2019) 1017–1020.
[4] S. Amaike, N.P. Keller, Annu. Rev. Phytopathol. 49 (2011) 107–133.
[5] Q. Li, Z. Lu, X. Tan, et al., Biosens. Bioelectron. 97 (2017) 59–64.
[6] L. Yu, Y. Zhang, C. Hu, et al., Food Chem. 176 (2015) 22–26.
[7] C.R. Armendáriz, Á.J.G. Fernández, M.C.L.R. Gironés, et al., Mycotoxins, Academic Press, Oxford, 2014.
[8] J. Fang, H. Yin, Z. Zheng, et al., Biol. Trace Elem. Res. 181 (2018) 142–153.
[9] W.S. Khayoon, B. Saad, C.B. Yan, et al., Food Chem. 118 (2010) 882–886.
[10] Y.M. Younis, K.M. Malik, Kuwait J. Sci. Eng. 30 (2003) 79–93.
[11] J.J.M. Xavier, V.M. Scussel, Int. J. Environ. Anal. Chem. 88 (2008) 425–433.
[12] Q. Zhou, D. Tang, Trends Anal. Chem. 124 (2020) 115814.
[13] W. Jiang, Z. Wang, G. Nölke, et al., Food Anal. Method 6 (2013) 767–774.
[14] L. Anfossi, G. d'Arco, M. Calderara, et al., Food Addit. Contam. 28 (2011) 226–234.
[15] Y.J. Sheng, S. Eremin, T.J. Mi, et al., Biomed. Environ. Sci. 27 (2014) 126–129.
[16] Y. Lin, Q. Zhou, D. Tang, et al., Anal. Chem. 89 (2017) 5637–5645.
[17] Y. Lin, Q. Zhou, Y. Lin, et al., Anal. Chem. 87 (2015) 8531–8540.
[18] S. Oh, J. Kim, V.T. Tran, et al., ACS Appl. Mater. Interfaces 10 (2018) 12534–12543.
[19] J. Chen, H. Xue, Q. Chen, et al., Chin. Chem. Lett. 30 (2019) 1631–1634.
[20] H. Shi, T. Jin, J.W. Zhang, et al., Chin. Chem. Lett. 31 (2020) 155–158.
[21] Y. Chen, Y. Xianyu, Y. Wang, et al., ACS Nano 9 (2015) 3184–3191.
[22] H. Chen, Z. Fang, Y. Chen, et al., ACS Appl. Mater. Interfaces 9 (2017) 39953–39961.
[23] S. He, L. He, B. Liu, et al., Chin. Chem. Lett. 30 (2019) 1031–1034.
[24] Y. Tang, W. Lai, J. Zhang, D. Tang, Microchim. Acta 184 (2017) 2387–2394.
[25] Y. Li, Y. Zhang, F. Li, et al., Biosens. Bioelectron. 92 (2017) 33–39.
[26] M. Li, X. Huang, Y. Guo, et al., Chin. Chem. Lett. 28 (2017) 1453–1459.
[27] H. Wang, H. Rao, X. Xue, et al., Anal. Chim. Acta 1097 (2020) 222–229.
[28] X. Ye, L. Jin, H. Caglayan, et al., ACS Nano 6 (2012) 2804–2817.
[29] H. Rao, X. Xue, H. Wang, Z. Xue, J. Mater. Chem. C 7 (2019) 4610–4621.
[30] B.J. Zhang, Y.S. Xia, Chin. Chem. Lett. 30 (2019) 1663–1666.
[31] M. Li, J. Chen, J. Pan, et al., Chin. Chem. Lett. 30 (2019) 541–544.
[32] Y. Xiong, K. Pei, Y. Wu, et al., Sens. Actuators B: Chem. 267 (2018) 320–327.
[33] Z. Gao, K. Deng, X. Wang, et al., ACS Appl. Mater. Interfaces 6 (2014) 18243–18250.
[34] S. Xu, W. Ouyang, P. Xie, et al., Anal. Chem. 89 (2017) 1617–1623.
[35] Y. Lin, S. Xu, J. Yang, et al., Sens. Actuators B: Chem. 267 (2018) 502–509.
[36] J. Chen, A.A. Jackson, V.M. Rotello, S.R. Nugen, Small 12 (2016) 2469–2475.
[37] C. Zhang, A.X. Yin, R. Jiang, et al., ACS Nano 7 (2013) 4561–4568.
[38] F.S. Sabet, M. Hosseini, H. Khabbaz, et al., Food Chem. 220 (2017) 527–532.
[39] S. Hu, X. Dou, L. Zhang, et al., Toxicon 150 (2018) 144–150.
[40] R.M. Gell, I. Carbone, J. Microbiol. Methods 158 (2019) 14–17.